

3D modelling of non-uniform and turbulent flow in vertical slot fishways

J.F. Fuentes-Pérez^a✉, A.T. Silva^b; J.A. Tuhtan^c; A. García-Vega^d; R. Carbonell-Baeza^e; M. Musall^f;
and M. Kruusmaa^g

^aCentre for Biorobotics, Tallinn University of Technology, Akademia tee 15A, 12618 Tallinn, Estonia.
juan.fuentes@ttu.ee; Fax: +3726202020; Tel.: +34618315468

^bNorwegian Institute for Nature Research (NINA), P.O. Box 5685 Sluppen, NO-7485 Trondheim, Norway.
ana.silva@nina.no

^cCentre for Biorobotics, Tallinn University of Technology, Akademia tee 15A, 12618 Tallinn. jef-
frey.tuhtan@ttu.ee

^dDepartment of Hydraulics and Hydrology, University of Valladolid, Avenida de Madrid 44, Campus La Yutera,
34004 Palencia, Spain. ana.garcia.vega@iaf.uva.es

^eInstitute of Water and River Basin Management, Karlsruhe Institute of Technology, P.O. Box 6980 76049 Karls-
ruhe, Germany. ruthcarbonellbaeza@gmail.com

^fInstitute of Water and River Basin Management, Karlsruhe Institute of Technology, P.O. Box 6980 76049 Karls-
ruhe, Germany. mark.musall@kit.edu

^gCentre for Biorobotics, Tallinn University of Technology, Akademia tee 15A, 12618 Tallinn, Estonia.
maarja.kruusmaa@ttu.ee

Abstract

Global stocks of freshwater fish have been on the decline for decades, driven in part by the obstruction of their migration routes by anthropogenic barriers. To mitigate such impacts, fishways have been developed to facilitate bidirectional fish migration. These structures are affected by the hydrological variability of rivers, which can cause changes in the up and downstream boundary conditions of fishways, leading to non-uniform hydraulic performance. Current methodologies in fishway design and analysis often assume uniform performance, most commonly relying on 1D approximations of the water level distribution. In this study we highlight the necessity of considering non-uniform performance. We provide an in-depth analysis methodology for non-uniform conditions, demonstrating the necessity of 3D models to correctly characterize non-uniformity and leveraging the synergy between 1D and 3D models. For this VOF method together with two turbulence modelling technics, RANS Standard k- ϵ and LES Smagorinsky models, are analyzed using OpenFOAM CFD platform.

Keywords: Fishways; CFD; RANS; LES; OpenFOAM; Hydraulic design; Non-uniform performance.

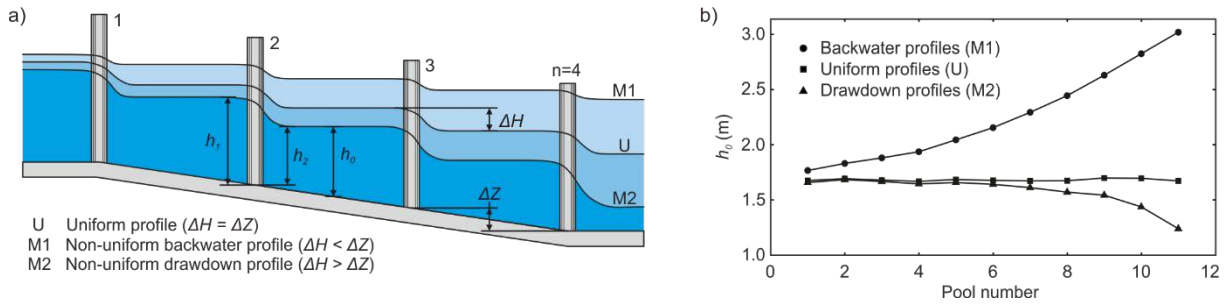
34 **1. Introduction**

35 River fragmentation caused by man-made structures is a major driver of ecological disruption
36 in aquatic systems, as it limits the free movement of freshwater organisms (Branco et al., 2012;
37 Nilsson et al., 2005). The current focus of restoration science is to reestablish connectivity of
38 regulated river systems. Considerable efforts have been devoted to the development and im-
39 provement of fish passage structures, in order to define design criteria adequate to the migration
40 requirements of multiple species and life-stages. Pool type fishways are the most popular alter-
41 native to allow free bidirectional movement of fish (Clay, 1995; FAO/DVWK, 2002; Fuentes-
42 Pérez et al., 2016; Larinier, 2002a). This type of hydraulic structures consists of consecutive
43 pools separated by cross-walls arranged in a stepped pattern, equipped with slots, weirs or ori-
44 fices, which are used by the fish to move from pool to pool. These structures aim to facilitate
45 fish passage by reducing the total height of the obstacle (H) into a series of smaller drops (ΔH)
46 providing compatible hydraulic conditions (e.g. velocity, turbulence level, power dissipation or
47 flow distribution) with the fish biomechanics skills.

48 In the past years, studies have been focusing in understanding the impact of hydraulics on fish
49 behavior and swimming capability within fishways. This analysis is commonly simplified by
50 assuming uniform flow regimes within the fishway, where ΔH is equal to the topographic dif-
51 ference between pools (ΔZ) (i.e. same water depth in all pools) (Bermúdez et al., 2010; Cea et
52 al., 2007; Puertas et al., 2012, 2004; Rajaratnam et al., 1992, 1986; Tarrade et al., 2011; Wu et
53 al., 1999). However, all constructed fishways are subject to the hydrological variability of the
54 rivers they are connected to, and thus uniformity is seldom observed under natural conditions
55 (Fuentes-Pérez et al., 2016; Marriner et al., 2016). Non-uniform regimes cause a range of dif-
56 ferent drops between all pools ($\Delta H \neq \Delta Z$) and the varied hydraulic conditions may lead to sig-
57 nificant differences in the passage efficiency (defined as the percentage of fish which entered
58 and successfully moved through a fishway) observed under uniform conditions (Fig. 1).

59

60



61

62 **Fig. 1.** Example of uniform and non-uniform profiles in a stepped fishway. h_0 is the mean water level in
63 the pool, h_1 is the mean water depth upstream and h_2 is the mean water depth downstream. a) Diagram
64 showing the possible profiles. b) Experimental results of Rajaratnam et al. (1986). (2 column)

65 Non-uniform performance will produce different mean water levels (h_0) between the pools of a
66 fishway, in idealized conditions manifested as a progressive decrement or increment of h_0 -
67 distribution [Fig. 1(a)]. These profiles were named by Rajaratnam et al. (1986) comparing the
68 distribution generated by h_0 in pools to the water profiles provided by the Bakhmeteff-Chow
69 method [Fig. 1(b)], resulting in two mean non-uniform water level distributions: backwater
70 (M1) and drawdown (M2) profiles (Fig. 1). M1 profiles are generated by the decrease of head-
71 water or the increase of tailwater levels, producing higher h_0 and lower drops ($\Delta H < \Delta Z$) in the
72 downstream pools. Conversely, M2 profiles are produced when the headwater level increases
73 or the tailwater level decreases, generating lower h_0 and higher drops ($\Delta H > \Delta Z$) in the down-
74 stream pools (Fuentes-Pérez et al., 2016). Furthermore, depending on the complexity of the
75 design (e.g. mixed cross-wall connections, different slopes or direction changes) both profiles
76 can appear mixed.

77 The modification of h_0 and ΔH profiles (Fig. 1) may have direct consequences on fishways
78 efficiency, as these variables have the potential to alter the spatial distribution and magnitude
79 of velocity and turbulence fields (Tarrade et al., 2008; Wu et al., 1999). Turbulence has a direct
80 impact on fish behavior, due to its influence on fish locomotion (Lupandin, 2005), fish stability
81 (Silva et al., 2012), as well as on path selection (Goettel et al., 2015). Elevated turbulence has
82 also been found to increase energy expenditure of swimming fish (Enders et al., 2005, 2003;
83 Guiny et al., 2005). Likewise, high turbulence levels can alter the detection of walls and avoid-
84 ance of other hazards, causing bodily damage of fish and in drastic situations leading to fish
85 mortality (e.g. impingement and entrance in intakes of hydropower stations) (Odeh et al., 2002).
86 Furthermore excessive ΔH will produce high velocities and turbulent levels which may limit
87 the entrance or passage of fish (Larinier, 2002a).

88 Thus, it is possible to account for possible misinterpretation of fish behavior by under or over-
89 estimate of fishway efficiency when assuming that fishways run only under uniform regime.
90 Therefore, it is imperative to study non-uniform conditions in fishways to improve the
91 knowledge of the local hydrodynamics under field conditions. Few studies have analyzed the
92 non-uniform regime within a fishway at one dimensional (1D) level (water level) (Fuentes-
93 Pérez et al., 2017, 2014; Krüger et al., 2010; Marriner et al., 2016). Nonetheless, the hydrody-
94 namics of non-uniform conditions within a fishway is a complex phenomenon that produces
95 alterations of the flow at a three-dimensional (3D) level, and should be taken into consideration.

96 In order to analyze and to understand the consequences of non-uniformity flow within fishways
97 for bidirectional passage of fish, as well as to demonstrate the feasibility of modelling this hy-
98 draulic situation, in this work 3D modelling of vertical slot fishways (VSF) was studied under
99 uniform and non-uniform conditions. This was accomplished using OpenFOAM, an open
100 source computational fluid dynamics (CFD) software (Greenshields, 2015). The unsteady flow
101 was simulated using the volume of fluid (VOF) method (interFoam solver) with two different
102 turbulence modelling techniques: (1) Reynolds-averaged Navier-Stokes (RANS) method using
103 standard $k-\epsilon$ model, which is a benchmark in fishway studies (Barton et al., 2009; Cea et al.,
104 2007; Khan, 2006; Marriner et al., 2016, 2014; Xu and Sun, 2009), and (2) large eddy simula-
105 tion (LES) method using the Smagorinsky turbulence model, which has demonstrated, in some
106 cases, better simulation performance of turbulence parameters than RANS (Van Balen et al.,
107 2010; Vuorinen et al., 2015). The numerical model results were compared to measured data
108 from an acoustic Doppler velocimeter (ADV) in a laboratory fishways model.

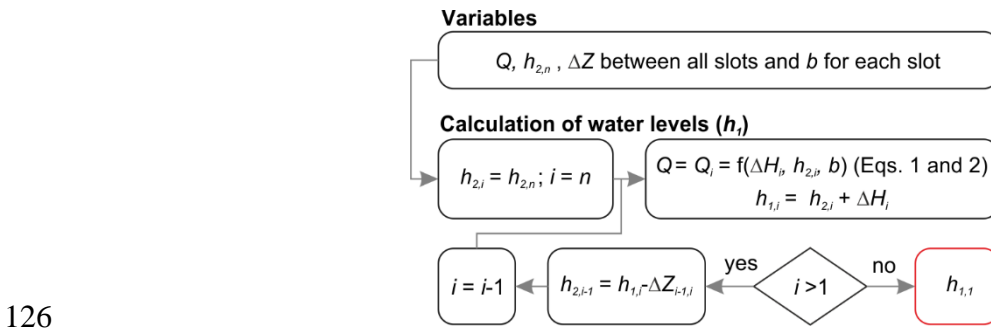
109 The main goals of our work were to: (1) show the effect of non-uniformity in VSFs in the 3D
110 domain; (2) validate 3D modelling results for non-uniform conditions comparing them with
111 measured data; (3) illustrate the use of 1D models to define boundary conditions for 3D models;
112 and (4) highlight the necessity of considering non-uniform performance to adapt fishways hy-
113 drodynamics to the requirements of target species.

114 **2. Numerical models**

115 **2.1. 1D model**

116 1D numerical methods are the benchmark for simulating non-uniformity in stepped fishways.
 117 However, these methods tend to oversimplify the underlying physics of flow field, as they pro-
 118 vide an average estimation of the mean water levels of each of the pool of the fishways, ne-
 119 glecting the vertical and horizontal spatial distribution of the flow.

120 Water levels are calculated via an iterative bottom-up calculus considering the boundary con-
 121 ditions of the system, which are the discharge through the fishway (Q) or the headwater level
 122 upstream ($h_{1,1}$) and tailwater level ($h_{2,n}$, where n corresponds to the total number of cross-walls
 123 in the fishway) (Fig. 1), the discharge equations involved in cross-walls (Fuentes-Pérez et al.,
 124 2014) and the basic geometrical parameters of the fishway [in case of VSF: ΔZ and slot width
 125 (b)] (Fig 2).



126
127 **Fig. 2.** Workflow of the iterative bottom-up calculation. (1 column)

128 The main component in the workflow are the discharge equations, as they must be able to cal-
 129 culate discharge correctly during different hydrodynamic scenarios. In this regard, it is possible
 130 to predict accurately uniform and non-uniform performances using Poleni's discharge equation
 131 (Eq. 1) (Poleni, 1717) together with Villemonte's submergence coefficient (C_V) (Eq. 2)
 132 (Villemonte, 1947). This has been demonstrated in the most common type of stepped fishways
 133 (vertical slot, pool and weir and step-pool nature-like fishways), in both field and laboratory
 134 conditions (Fuentes-Pérez et al., 2017, 2014).

135
$$Q = \frac{2}{3} \cdot C_V \cdot b \cdot h_1^{1.5} \cdot \sqrt{2 \cdot g} \quad (1)$$

136
$$C_V = \beta_0 \cdot \left[1 - \left(\frac{h_2}{h_1} \right)^{1.5} \right]^{\beta_1} \quad (2)$$

137 Where g stands for the acceleration due gravity (9.81 m²/s) and β_0 and β_1 are coefficients which
138 depend on the geometry of the flow control structure in the cross-wall.

139 The bottom up calculation of the water level can be calculated manually using the defined al-
140 gorithm (Fig 2) or by implementing it in the desired program. Once the water levels are calcu-
141 lated, it is possible to derive more complex information, such as maximum velocity in the slot
142 [$u_{\max} = \sqrt{2 \cdot g \cdot \Delta H}$ (Rajaratnam et al., 1986)] or the volumetric power dissipation in the pool [
143 $VPD = Q \cdot \Delta H \cdot g \cdot \rho / (h_0 \cdot B \cdot L)$, where ρ is the water density (1000 kg/m³), B is the pool width
144 and L the pool length (FAO/DVWK, 2002)].

145 **2.2. 3D model**

146 In order to reach a complete characterization of the non-uniformity phenomena and analyze its
147 real consequences, 3D models seem to be an interesting alternative, as they have the potential
148 of simulating any variable of interest as well as reproducing its performance over time.

149 In this study the 3D model is implemented using the open source numerical code OpenFOAM
150 (release 3.0.1) (Greenshields, 2015). OpenFOAM is a C++ toolbox that uses a tensorial ap-
151 proach and finite volume method (FVM) for the resolution of continuum mechanics problems,
152 including CFD (Weller et al., 1998).

153 The resolution of transient flow of two fluids separated by a sharp interface can be achieved
154 with the prebuilt Eulerian solver interFoam (Ubbink, 1997), which is an implementation of the
155 classical VOF method (Hirt and Nichols, 1981) and uses the PIMPLE algorithm (Higuera et al.,
156 2013) for the pressure-velocity coupling.

157 **2.2.1. Flow equations**

158 For the description of the 3D system under study [incompressible ($\rho = \text{constant}$) and isother-
159 mal] the Navier-Stokes equations in their incompressible form are used [Eqs. 3 (continuity
160 equation) and 4 (momentum equation)] (Bayon et al., 2016; Ubbink, 1997).

$$161 \quad \nabla \bar{u} = 0 \quad (3)$$

$$162 \quad \frac{\partial \bar{u}}{\partial t} + \bar{u} \cdot \nabla \bar{u} = -\frac{1}{\rho} \nabla p + \nu \nabla^2 \bar{u} + \bar{f}_b \quad (4)$$

163 where p is the pressure, ν is the kinematic viscosity, \bar{f}_b are the body forces (g) and t is the time.

164 The coexistence of the two immiscible fluids [named as water (1) and air (2)] involved in the
165 relation is managed by VOF method, where the volume fraction α defines the portion in each
166 mesh element occupied by the different fluids (Hirt and Nichols, 1981) ($\alpha = 1$ when is occupied
167 by water, $0 < \alpha < 1$ in the interface and $\alpha = 0$ for air). Considering this, the transport of α in
168 time is expressed by:

$$169 \quad \frac{\partial \alpha}{\partial t} + \nabla \cdot (\bar{u} \alpha) = 0 \quad (5)$$

170 Other properties (ϕ) are treated as a weighted mixture of both fluids in each mesh element:

$$171 \quad \phi = \phi_1 \alpha + \phi_2 (1 - \alpha) \quad (6)$$

172 Consequently, a set of values from 0 to 1 are obtained without an explicit interface between
173 fluid. In this sense, to define a fluid interface ($\alpha = 0.5$) and to avoid the use of interface recon-
174 struction schemes (Lopes et al., 2016), interFoam adds an artificial compression term
175 $\nabla \cdot [\bar{u}_c \alpha (1 - \alpha)]$ [where \bar{u}_c is the vector of relative velocity between the two fluids or, compres-
176 sion velocity (Berberović et al., 2009)] to the left side of Eq. 5.

177 **2.2.2. Turbulence modelling**

178 Local hydrodynamic conditions within a VSFs are characterized by intermittent, large and
179 small-scale fluctuations in vorticity, pressure and velocity. Thus, the modelling of these fluctu-
180 ations is essential for correct calculation (Bombač et al., 2014) and has demonstrated to be an
181 extremely important factor in the characterization and evaluation of the performance of fish-
182 ways for fish passage (Silva et al., 2011).

183 Although turbulence can be numerically resolved in its different scales using direct numerical
184 simulations (DNS), it is too computationally demanding (Blocken and Gualtieri, 2012). Thus,
185 to solve a computationally manageable problem, RANS and LES methods are the most reason-
186 able alternatives.

187 The majority of studies have implemented RANS methods as numerical technique for the 3D
188 modelling of VSF (Barton et al., 2009; Cea et al., 2007; Khan, 2006; Marriner et al., 2016,
189 2014, among others). This is due to their proven application in a wide range of flows (Bombač
190 et al., 2014) as well as their agreement in time-averaged or ensemble-averaged velocity distri-
191 bution predictions compared to experimental data (Barton et al., 2009; Cea et al., 2007;

192 Marriner et al., 2014). In general, RANS methods have shown that they are capable of providing
193 a compromise between accuracy and computational cost (Blocken and Gualtieri, 2012;
194 Vuorinen et al., 2015). However a major setback in using RANS is that the approach only re-
195 solves mean flow characteristics (Blocken and Gualtieri, 2012) largely neglecting the more
196 rapid turbulent structures in the flow. These effects are modeled in RANS using simplifying
197 equations which limit their results in highly dynamic flows (Pope, 2001).

198 Due to the higher computational demand, there are few studies using 3D LES models in VSFs
199 (Klein and Oertel, 2015; Musall et al., 2015; Oberle et al., 2012). In contrast to RANS, LES
200 includes large-scale turbulent velocity fluctuations, and provides time resolved flow fields in-
201 cluding turbulent structures. This is achieved by spatial filtering; large scale eddies are included
202 in the numerical solver whereas smaller ones are modelled semi-empirically. Thus the results
203 of LES are usually closer to those of DNS (Zhang et al., 2014) and they have the potential of
204 more accurately resolving the turbulence parameters. Nonetheless, LES methods typically re-
205 quire higher mesh spatial resolution (Pope, 2001) and thus, they are more computationally de-
206 manding. The final resolved scale of any given model depends on the grid size of the mesh,
207 never achieving a mesh independent solution (Celik et al., 2009).

208 Due to the pros and cons of both methods, in the present work both RANS and LES have been
209 compared. The RANS method has been evaluated by means of the Standard k - ε model (Furbo,
210 2010; Launder and Spalding, 1974) and the LES method using the Smagorinsky model
211 (Deardorff, 1970; Smagorinsky, 1963).

212 *Standard k - ε model*

213 The turbulence k - ε model, is based on the substitution of ν by the effective viscosity (ν_{eff}) (Eq.
214 7) in the momentum equation, where ν_{eff} is a modeled viscosity that takes into account the
215 transport and dissipation of energy caused by the velocity fluctuations.

$$216 \quad \nu_{eff} = \nu + \nu_t \quad (7)$$

217 ν_t is the turbulent viscosity and it is expressed in terms of the turbulent kinetic energy (k) and
218 the dissipation rate (ε) (Eq. 8):

$$219 \quad \nu_t = C_v \frac{k^2}{\varepsilon} \quad (8)$$

220 In order to estimate k and ε , their transport equations are solved:

$$221 \quad \frac{\partial k}{\partial t} + \bar{u}_j \frac{\partial k}{\partial x_j} - \frac{\partial}{\partial x_j} \left(\nu + \frac{\nu_t}{\sigma_k} \right) \left(\frac{\partial k}{\partial x_j} \right) = \nu_t \frac{\partial \bar{u}_i}{\partial x_j} \left(\frac{\partial \bar{u}_i}{\partial x_j} - \frac{\partial \bar{u}_j}{\partial x_i} \right) - \varepsilon \quad (9)$$

$$222 \quad \frac{\partial \varepsilon}{\partial t} + \bar{u}_j \frac{\partial \varepsilon}{\partial x_j} - \frac{\partial}{\partial x_j} \left[\left(\nu + \frac{\nu_t}{\sigma_\varepsilon} \right) \frac{\partial \varepsilon}{\partial x_j} \right] = C_1 \frac{\varepsilon}{k} \nu_t \frac{\partial \bar{u}_i}{\partial x_j} \left(\frac{\partial \bar{u}_i}{\partial x_j} - \frac{\partial \bar{u}_j}{\partial x_i} \right) - C_2 \frac{\varepsilon^2}{k} \quad (10)$$

223 where x_i and x_j are Cartesian space coordinates and u_i, u_j are the mean velocity components in
 224 direction x_i and x_j , respectively. Regarding $C_\nu, C_1, C_2, \sigma_k$ and σ_ε , they are model parameters
 225 whose values can be found in Launder and Spalding, 1974 (Table 1).

226 **Table 1.** Values of the constant model parameters in the k - ε model (Launder and Spalding, 1974). (1
 227 column)

C_ν	C_1	C_2	σ_k	σ_ε
0.09	1.44	1.92	1.00	1.30

228

229 *Smagorinsky model*

230 In the case of Smagorinsky model, similarly to k - ε model, an effective viscosity is defined:

$$231 \quad \nu_{eff} = \nu + \nu_{sgs} \quad (11)$$

$$232 \quad \nu_{sgs} = C_k \Delta \sqrt{k} \quad (12)$$

233 Where ν_{sgs} is the subgrid-scale kinematic viscosity (Eq. 12) and Δ is the filter width (defined
 234 as the cube root volume of each cell). Note that k is not solved by a transport equation but rather
 235 it is calculated from the velocity field (Eq. 13).

$$236 \quad k = \frac{C_k}{C_e} \Delta^2 |\bar{S}|^2 \quad (13)$$

$$237 \quad \nu_{sgs} = C_k \sqrt{\frac{C_k}{C_e}} \Delta^2 |\bar{S}| = C_s \Delta^2 |\bar{S}| \quad (14)$$

238 where $|\bar{S}| = \sqrt{2 \cdot S_{ij} S_{ij}}$ and S_{ij} is the rate of strain of the large scale or resolved field. C_k and C_e
 239 are both model constants (Table 2), which are related with the classical Smagorinsky constant
 240 (C_s) (Eq. 14).

241 **Table 2.** Values of the constant model parameters in the Smagorinsky model (Deardorff, 1970; Lilly,
 242 1966; Sidebottom et al., 2015). (1 column)

C_k	C_e	C_s
0.094	1.048	0.168

243

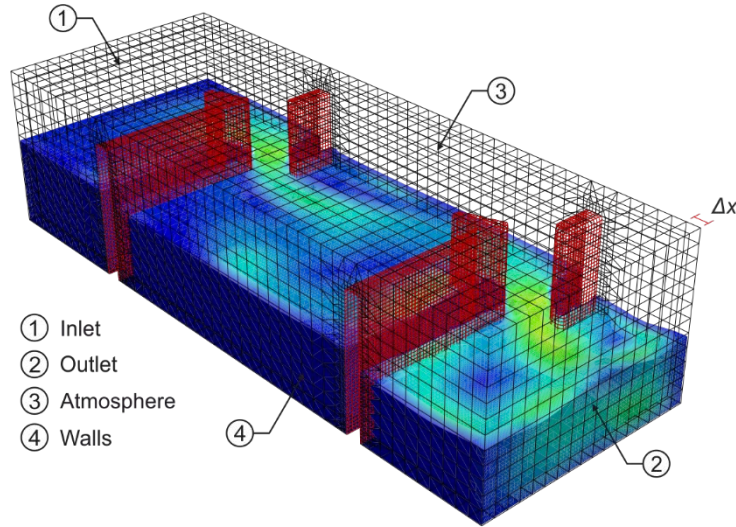
244 **2.2.3. Spatial and temporal discretization**

245 The problem under study consists of a sloped channel divided by cross-walls of differing shape
 246 depending on the type of VSF under study. These complex geometries make it challenging to
 247 apply structured meshes. For this reason, all studied meshes were generated in this work using
 248 a two-step procedure. First, the blockMesh utility (Greenshields, 2015) was used to create a
 249 simple fully structured hexahedral mesh of the channel without considering the cross-walls,
 250 defining cubic element of size Δx (Fig. 3). After, using the structured mesh as a base, the snap-
 251 pyHexMesh utility (Greenshields, 2015) was applied to create a high quality hex-dominant
 252 mesh based on the VSF cross-wall definition (Fig. 3). In all studied cases the surface refine-
 253 ments (Jackson, 2012) were defined to obtain a suitable dimensionless wall distance (y^+)
 254 (Section 2.2.4).

255 The final choice of mesh element size is highly case specific (Bayon et al., 2016). Therefore, a
 256 mesh sensitivity analysis was performed according to the American Society of Mechanical En-
 257 gineers (ASME) criteria (Celik et al., 2008) to study the influence of Δx (Section 4).

258 Time discretization was dynamically controlled using the Courant number (Cr) as threshold. In
 259 this sense, OpenFOAM uses a semi-implicit variant of the Multidimensional Limiter for Ex-
 260 plicit Solution (MULES) with an operator splicing procedure to solve the transport equation of
 261 the phase fraction (Greenshields, 2015). In this way the convergence is possible with larger Cr
 262 than usual (usually $Cr \leq 1$) (Mooney et al., 2014). Thus, a Cr threshold of 6 was used until
 263 convergence (evaluated by monitoring the evolution of inlet-outlet discharge rate and mean
 264 water depth (h_0) stability in all the pools) and then, Cr was decreased to 1 to report the final
 265 results.

266



267

268 **Fig. 3.** An example of a mesh generated by the two steps procedure ($\Delta x = 0.1$ m) including all boundary
 269 surfaces. (1 column)

270 2.2.4. Boundary conditions

271 Table 3 summarizes the boundary conditions (BC) for the four different types of boundaries
 272 defined: inlet, outlet, atmosphere and walls (Fig. 3). A detailed explanation of the boundary
 273 types and their definitions can be found in the NEXT Foam (2014) or openFoam (2016) litera-
 274 ture.

275 **Table 3.** Boundary conditions used for the problem definition in OpenFOAM. An extended definition
 276 of their numerical implementation can be found in NEXT Foam (2014) or openFoam (2016). (2 column)

Boundary	α	u	p	RANS		LES
				k	ϵ	ν_t
Inlet	<i>variableHeight-FlowRate</i>	<i>variableHeight-FlowRateInletVelocity</i>	<i>fixedFlux-Pressure</i>	<i>fixedValue</i>	<i>fixedValue</i>	<i>Calculated</i>
Outlet	<i>zeroGradient</i>	<i>outletPhaseMeanVelocity</i>	<i>fixedFlux-Pressure</i>	<i>inletOutlet¹</i>	<i>inletOutlet¹</i>	<i>Calculated</i>
Atmosphere	<i>inletOutlet¹</i>	<i>pressureInletOutletVelocity</i>	<i>totalPressure</i>	<i>inletOutlet¹</i>	<i>inletOutlet¹</i>	<i>Calculated</i>
Walls	<i>zeroGradient</i>	<i>fixedValue²</i>	<i>fixedValue²</i>	<i>kqRWall-Function³</i>	<i>epsilonWall-Function</i>	<i>nutkWall-Function</i>

¹Generic outflow condition (zero-gradient), with specified inflow for the case of return flow; ²No-Slip condition
³Enforces a zero-gradient condition.

277

278 The overall performance of each scenario was controlled by defining a constant flow rate at the
 279 inlet (*variableHeightFlowRateInletVelocity*), enabling the free water level oscillation (*variableHeightFlowRate*) and a constant mean velocity in the outlet (*outletPhaseMeanVelocity*). All
 280

281 of them correspond to mixed BCs. Pressure BCs at the inlet and outlet were set to *fixedFlux-*
282 *Pressure*, which adjusts the pressure gradient such that the flux on the boundary is specified by
283 the velocity BC (Neumann BC). At the walls, a no slip condition was imposed. The upper sur-
284 faces of the mesh, as they were exposed to atmospheric pressure were considered as a free
285 surface and should allow the flow to enter and leave the domain freely. This was achieved
286 defining an outflow condition for u [*pressureInletOutletVelocity* (Mixed BC)] and fixing the
287 value of the total pressure [*totalPressure* (Dirichlet BC)]. Likewise, at the inlet the boundary
288 values of k and ε were set to low constant values and allowed to develop within the fishway.

289 Regarding BCs of k , ε and ν_t in walls, they require a special treatment because of the viscous
290 flow region attached to physical bodies (Bayon et al., 2016). For k it was set to be *kqRWall-*
291 *Function* which simply acts as a Neumann BC, for ε it was set to be *epsilonWallFunction*, which
292 provides a condition for high Reynolds number turbulent flow cases (Furbo, 2010; NEXT
293 Foam, 2014) and, for ν_t , it was set to be *nutkWallFunction*, which provides a turbulent kine-
294 matic viscosity condition based on turbulent kinetic energy (Moukalled et al., 2016; NEXT
295 Foam, 2014). Likewise, roughness in walls was neglected given the small roughness of the
296 material used in the experimental setup (Section 3). Likewise, many studies have demonstrated
297 that wall friction does not play an important role in this type of flow (Barton and Keller, 2003;
298 Bombač et al., 2014; Cea et al., 2007)

299 The fundamental concept behind the use of wall functions is to apply them at some distance
300 from the wall so that the turbulence models can be solved correctly (Furbo, 2010). In this sense
301 the main requirement to apply these wall functions is that mesh elements in contact with solid
302 boundaries must have a dimensionless wall distance (y^+) [law of the wall (Von Kármán, 1931)]
303 between the buffer and the logarithmic sublayers (usually defined as $30 < y^+ < 300$) (Bayon et
304 al., 2016; Furbo, 2010) (for the final models a mean value of 132.58 ± 46.09 was obtained).

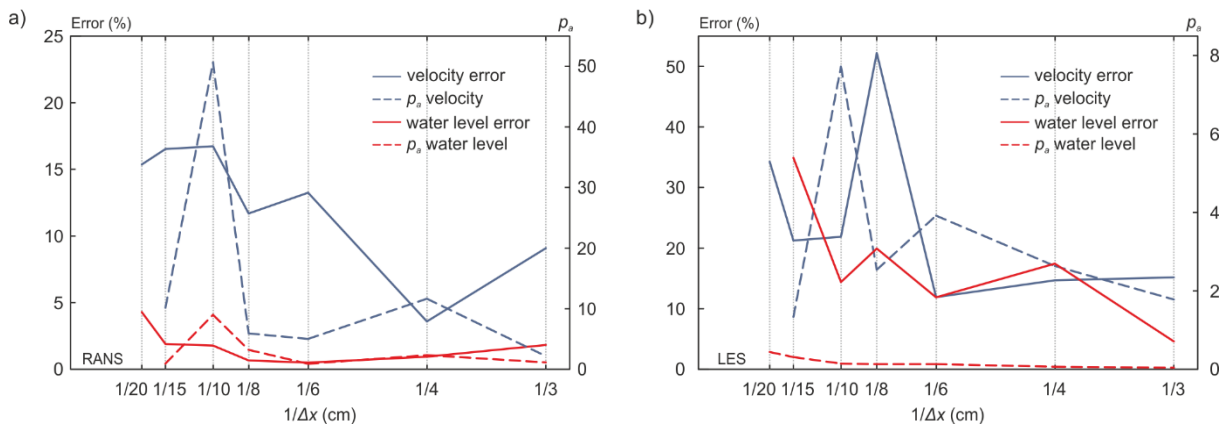
305 **3. Experimental setup**

306 The outcomes of the 3D numerical models were validated comparing the results to a laboratory
307 case study.

308 The laboratory data was collected from a scale model (1:1.6) of 2 pools and 3 cross-walls at
309 zero slope of a VSF situated in Koblenz (Germany) [Fig. 4(a)] (Musall et al., 2015). The ab-
310 sence of slope always provides a M2 profile [Fig. 1(a)] and is a typical solution chosen for small
311 obstacles exposed to high hydrological variability (Bice et al., 2017). The aim of this setup was

336 **4. Mesh and time sensitivity analysis**

337 The mesh sensitivity analysis was performed based on the ASME criteria (Bayon et al., 2016;
 338 Celik et al., 2008). The mesh size employed for the analysis were 0.20, 0.15, 0.10, 0.08, 0.06,
 339 0.04, 0.03 and 0.02 m, with the global refinement ratio of 10 (0.2/0.02) above of the recom-
 340 mended minimum value of 1.30 (Bayon et al., 2016; Celik et al., 2008). Fig. 5 shows the dif-
 341 ference in percentage between two consecutive mesh sizes as well as the apparent order (p_a) for
 342 average h_0 distribution in all pools and the mean of the average velocity distribution in the
 343 vertical axis in jet region (A in the Fig. 4), quiescent region (C in the Fig. 4) and shear layer (D
 344 in the Fig. 4) for both turbulence models.



345 **Fig. 5.** Summary of mesh sensitivity analysis for Koblenz VSF with $Q = 0.130 \text{ m}^3/\text{s}$. Distribution of
 346 errors between two consecutive mesh sizes and apparent order (Celik et al., 2008) for average h_0 distri-
 347 bution in all pools and average velocity distribution in selected regions for (a) RANS and (b) LES tur-
 348 bulence models. (2 columns)

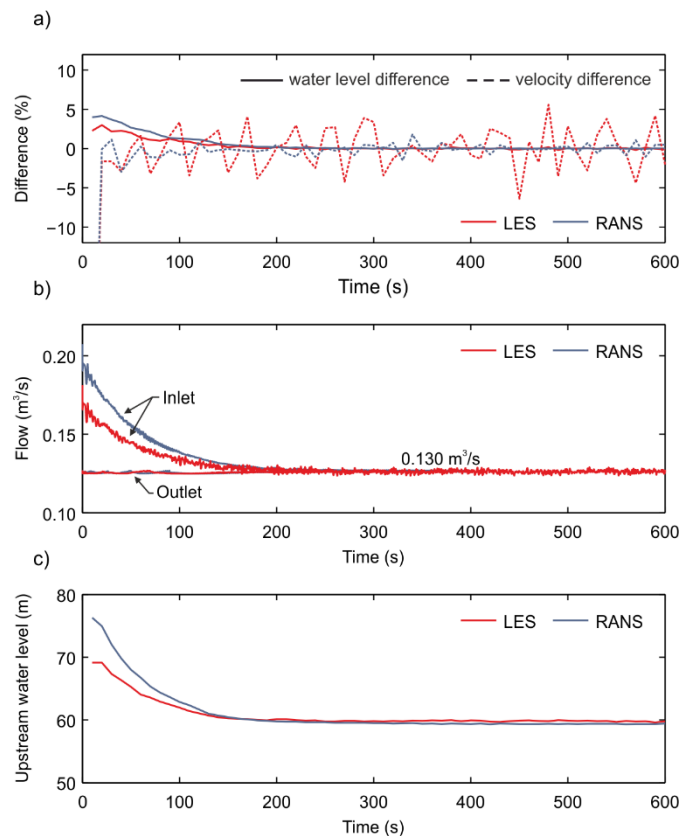
350 The observed apparent order distribution of the RANS model [Fig. 5(a)] demonstrates that os-
 351 cillatory convergence for velocity distribution was reached in sizes below 0.06 m (Celik et al.,
 352 2008). Likewise, the convergence of the water level was reached slightly faster (0.08 m) con-
 353 sidering the error distribution between meshes.

354 Regarding LES, it is important to mention that the Smagorinsky method is an implicit approach
 355 and thus the filter size will change with the selected grid size; as a result, there is no truly grid-
 356 independent solution. Thus the selected LES method approaches DNS if the grid size is refined
 357 (Celik et al., 2009). This can be seen in the observed error pattern which is continuously de-
 358 scending, especially when considering the velocity [Fig. 5(b)]. Nevertheless, for the case under
 359 study, the p_a distribution for h_0 below $\Delta x = 0.08 \text{ m}$ seemed to decelerate.

360 It was found that the best overall choice of mesh resolution was $\Delta x = 0.03$ m. This value was
 361 below the 0.06 m considered for RANS, and at the same time allows to study the potentiality
 362 of LES solutions using still a computationally manageable solution (number of cells =
 363 $1.08 \cdot 10^6$). In cases where only depth profile distributions were going to be considered, $\Delta x =$
 364 0.08 m seemed a reasonable grid size for both turbulence models.

365 The numerical uncertainty of the model was calculated after Celik et al. (2008), resulting in a
 366 mean value in the asymptotic range for LES 0.72% and 7.61%, and for RANS 1.27% and
 367 10.88% for h_0 distribution and velocity profile, respectively.

368 Despite the chaotic behaviour of flow, when simulation converged to a stable solution. The
 369 differences between time steps were reduced until they reach an oscillatory behaviour in all the
 370 variables (Fig. 6). This behaviour was monitored for all studied scenarios, and was visualized
 371 by plotting the difference between consecutive time steps for the hydraulic parameter within
 372 the fishway (e.g. mass flow, stability of global water levels, or stability of water level upstream)
 373 and choosing to end the simulation when an asymptotic behaviour was reached.



374

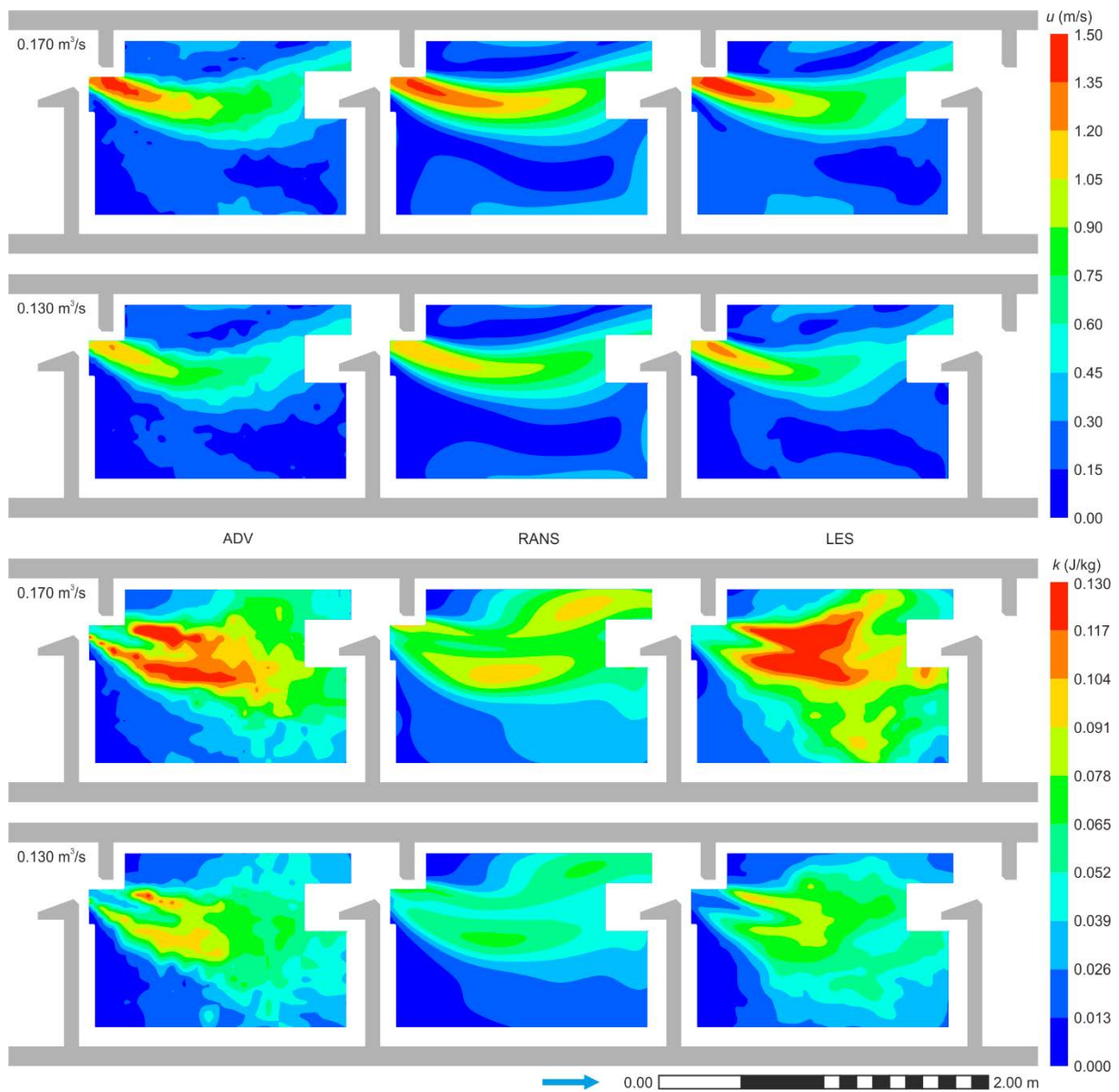
375 **Fig. 6.** Convergence to equilibrium for Koblenz VSF with a flow of $0.130 \text{ m}^3/\text{s}$. a) Average h_0 distribu-
 376 tion in all pools and average velocity differences in consecutive time steps. b) Evolution of volumetric
 377 flow in the inlet and outlet. c) Water level evolution in the inlet. (1 column)

378 **5. Results and Discussion**

379 **5.1. Turbulence model comparison**

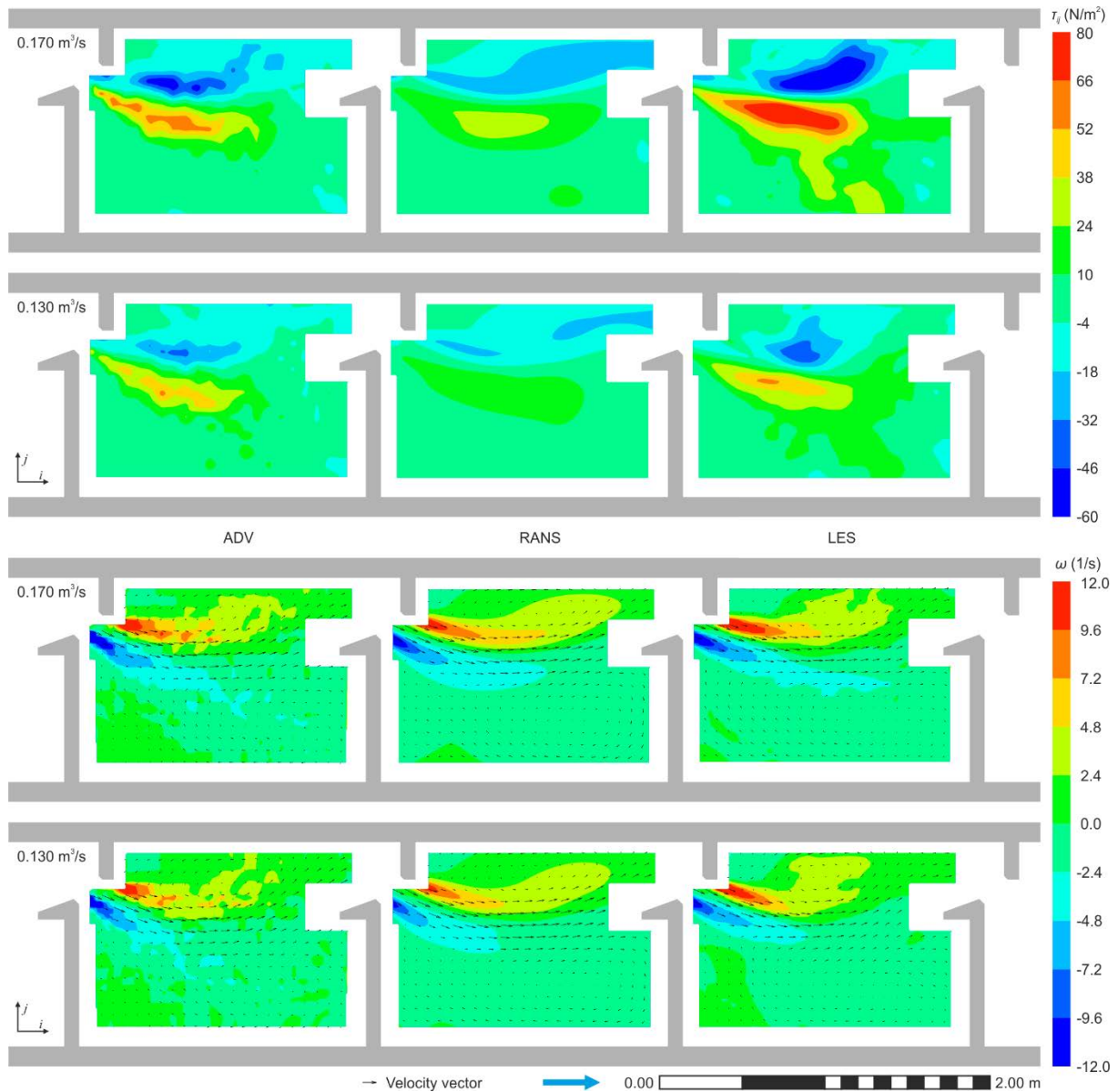
380 Figs. 7 and 8 show the hydrodynamics of the same Koblenz VSF pool subject to the different
381 boundary conditions simulated by means of the two turbulence models considered, as well as,
382 measured with the ADV. According to these figures both turbulence modelling techniques seem
383 able to simulate the spatial distribution of the considered hydrodynamic variables, accurately
384 in the cases of velocity (u in Fig.7) and the time averaged vorticity in the vertical plane (ω_{ij} in
385 Fig. 8) and, slightly overestimating (LES) or underestimating (RANS) in the case of turbulent
386 kinetic energy (k in Fig.7) and Reynold stress (τ_{ij} in Fig.8).

387



388

389 **Fig. 7.** Contour maps in the second pool for u and k (parallel to the bed plane at $0.60 \cdot h_0$) of the compar-
 390 ison of CFD models with measured data (ADV). Models are the average value of 60 s of simulation. (2
 391 columns)



392
 393 **Fig. 8.** Contour maps in the second pool for Reynold stress ($\tau_{ij} = -\overline{\rho u'_i u'_j}$) and time-averaged vorticity
 394 in the vertical plane ($\omega_{ij} = (\partial u_j / \partial x_i - \partial u_i / \partial x_j)$) (parallel to the bed plane at $0.60 \cdot h_0$) of the comparison
 395 of CFD models with measured data (ADV). Models are the average value of 60 s of simulation. (2
 396 columns)

397 Table 4 shows the numerical values [mean absolute error (MAE), root-mean-square error
 398 (RMS) and squared Pearson correlation (coefficient of determination, R^2)] of the profile com-
 399 parison and confirms numerically the observed in the profiles, u and ω_{ij} are the best estimated

400 variables. When the errors of both turbulence methods are compared, no significant differences
 401 are detected (t -test for two samples, significance level = 0.05, p -value = 0.363 for MAE and p -
 402 value = 0.246 for RMS). However, for the studied cases, LES method offers a significantly
 403 better linear correlation with respect to the ADV data (t -test for two samples, significance level
 404 = 0.05, p -value = 0.038), which seems to indicate an overall better spatial agreement with the
 405 measured data (for a graphical comparison check supplementary material, Fig. S1).

406 **Table 4.** Differences in u , k , τ_{ij} and ω_{ij} , between considered models and measured ADV profiles. A
 407 graphical summary of the table can be found in the supplementary figure, Fig. S1. (2 column)

Discharge (m ³ /s)	Variable	RANS			LES		
		MAE	RMS	R^2	MAE	RMS	R^2
0.170	u	0.070	0.085	0.931	0.056	0.075	0.936
	k	0.015	0.016	0.731	0.014	0.018	0.797
	τ_{ij}	6.077	7.205	0.729	10.045	13.899	0.745
	ω_{ij}	0.884	1.072	0.837	0.874	1.066	0.835
0.130	u	0.074	0.090	0.898	0.044	0.059	0.942
	k	0.014	0.013	0.675	0.008	0.011	0.804
	τ_{ij}	5.553	5.848	0.620	5.596	7.709	0.746
	ω_{ij}	0.807	0.971	0.810	0.733	0.950	0.814

408

409 In LES models, errors were higher at high discharge scenario, which may indicate that an in-
 410 crease of flow complexity due to a higher discharge may require a further refinement to obtain
 411 same error magnitudes. Nevertheless, at the studied level, the differences were not significant
 412 (t -test p -value = 0.372 for MAE and p -value = 0.379 for RMS).

413 In general, the observed errors are in accordance or smaller than other specialized references
 414 with numerical information about model validation. For instance, Marriner et al. (2014) ob-
 415 served a MAE for the u of 0.06 m/s and An et al. (2016) of 0.1 m/s, in both cases using RANS
 416 $k - \varepsilon$ model. In general, it is worth mentioning the difficulty of finding numerical validation
 417 data in the simulation studies of VSFs, moreover for turbulence metrics.

418 RANS methods are the usual alternative when modelling VSFs (Barton et al., 2009; Cea et al.,
 419 2007; Khan, 2006; Marriner et al., 2016, 2014) because: (1) RANS provides an easier way to
 420 select the mesh size as a mesh independent solution can be reached and (2) this solution may
 421 be found with a coarser mesh than LES. In this work, the suitable RANS mesh resolution was

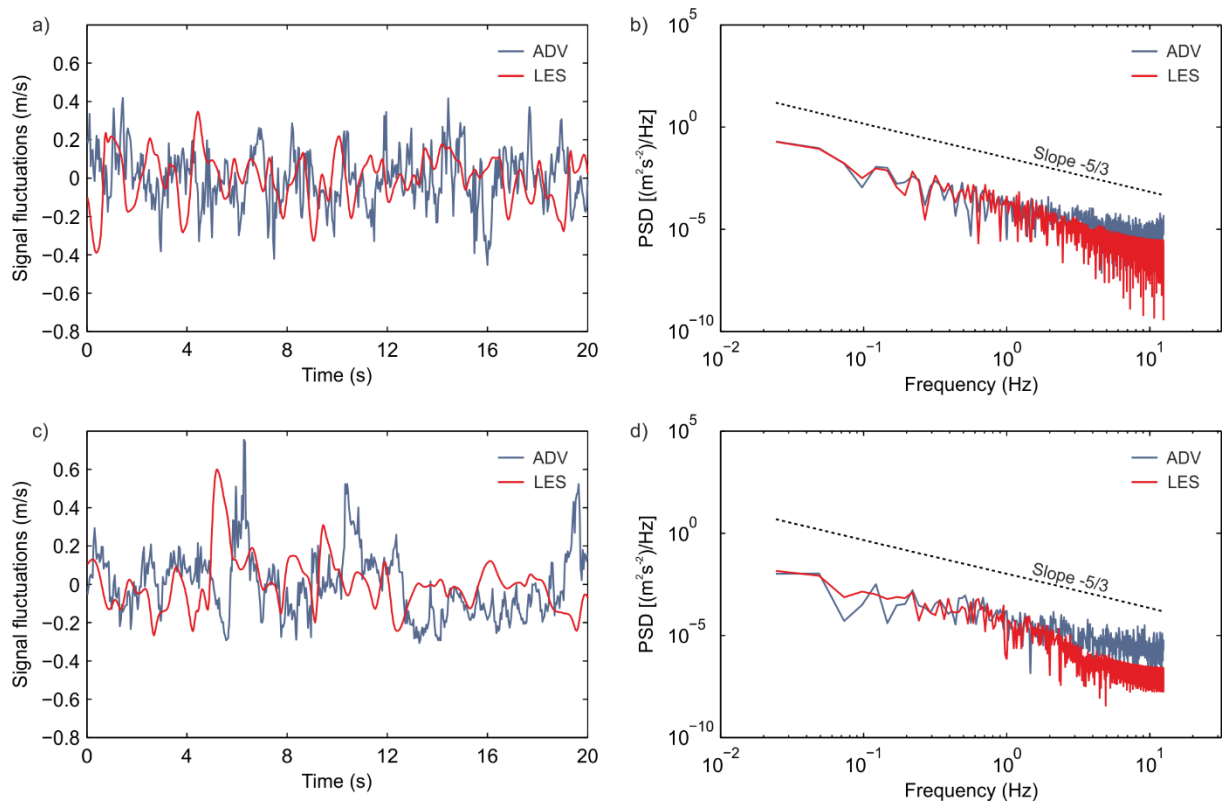
422 found to be $\Delta x = 0.06$ m for the studied cases (Section 4), which is also smaller than the mesh
423 sizes used in other studies (e.g. An et al., 2016; Marriner et al., 2014; Quaranta et al., 2016).

424 LES method was found to provide a small but significant improvement when compared with
425 the measured data under the considered model configuration. Likewise, further refinement may
426 further increase the accuracy, but this increase in accuracy always comes at the expense of
427 higher computational costs.

428 In contrast to RANS, in LES the larger eddies are explicitly resolved and the desired temporal
429 resolution can be reached. This has been identified as a “missing piece” of information in stud-
430 ies on fish swimming and turbulent flows and as imperative to a better understanding of the
431 relationship between fish behaviour and hydraulic conditions within a fishway (Silva et al.,
432 2012).

433 In this sense, Fig. 9 shows the velocity signal recorded by ADV faced to the one simulated by
434 LES model as well as their power spectral density in two different points [slot (A) and pool (B),
435 Fig. 4]. The magnitude of the velocity fluctuations is in accordance with measurements, how-
436 ever as pointed out in the methodology section, LES filters out high frequency oscillation ac-
437 cording to the size of the used cell size (Eq. 12). Fig 9(b) shows the difficulty of the model to
438 estimate the high frequency oscillations, which could be adjusted by adjusting cell size. Never-
439 theless, it is yet to be determined which fluctuations are relevant for fish.

440



441

442 **Fig. 9.** Velocity signal (25 Hz) measured by ADV and simulated by LES method in two spatially sepa-
 443 rated points of Koblenz VSF: slot (A Fig. 4) and pool (B Fig. 4). a) Raw signals in the slot. b) Power
 444 spectral density (*PSD*) of signals in the slot. c) Raw signals in the pool. d) Power spectral density of
 445 signals in the pool. (2 column)

446 Considering the results of the comparison between models and point velocity measurements,
 447 both turbulence models seem to provide acceptable results for the study case. Specifically, it
 448 was found that LES provided a closer spatial agreement with the measured data. As previously
 449 discussed, RANS can provide a mesh independent solution with coarser discretization which
 450 makes it a good candidate to simulate larger models. Nevertheless, the absence of the possibility
 451 in RANS of calculating the temporal fluctuations, makes LES more interesting for biological
 452 studies interested in smaller spatial and temporal scales, such as behavioural studies inside the
 453 pool. Thus, an integrated approach combining both turbulence models can be a good alternative,
 454 using RANS to simulate the global scenario and LES to focus in key smaller areas of interest.

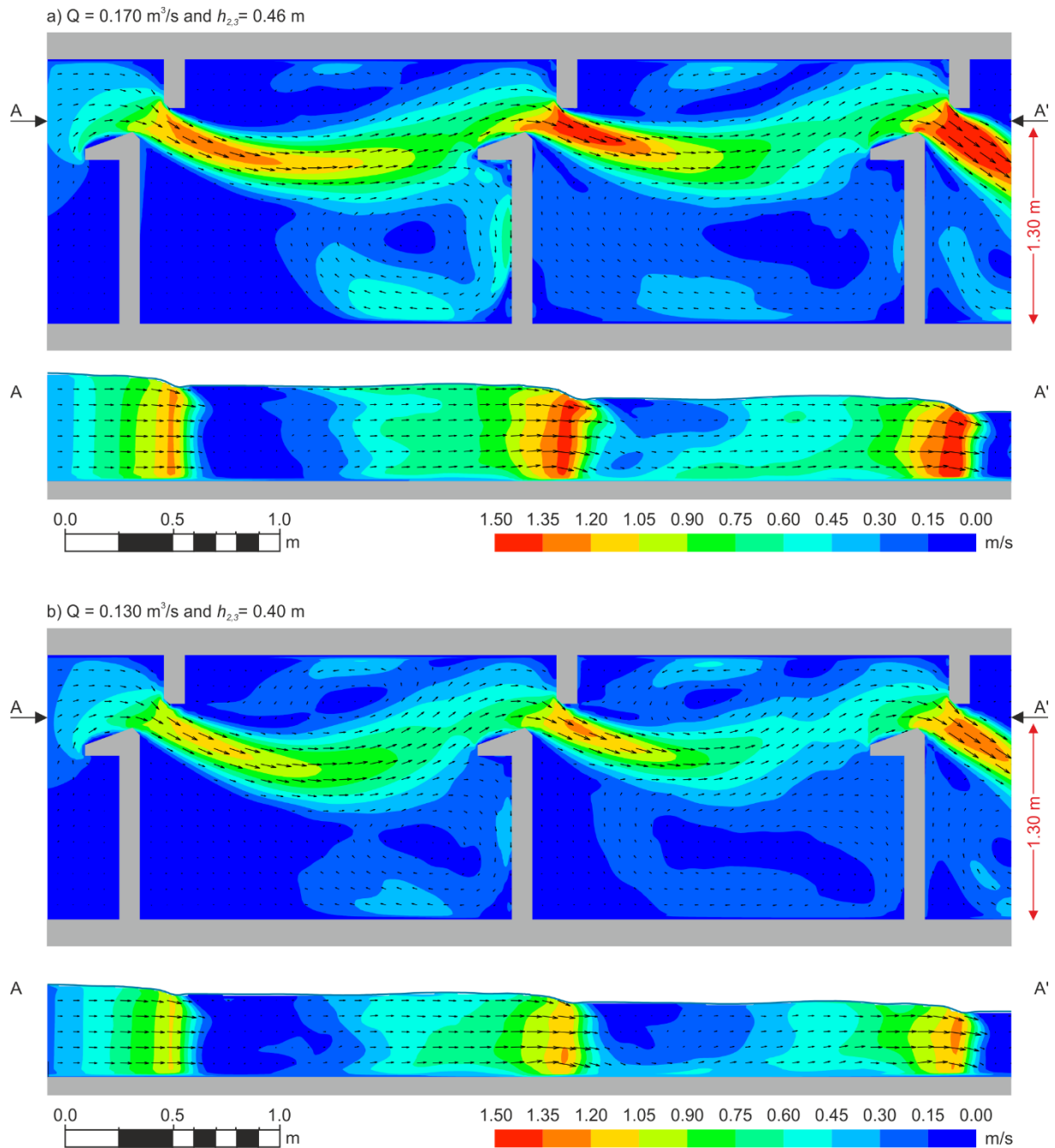
455 5.2. Non-uniformity

456 Different river scenarios will generate different boundary conditions, which in turns, will pro-
 457 duce different non-uniform performances in fishways, altering the distribution of h_0 in the pools
 458 as well as ΔH in slots to find a new equilibrium balance in the fishway (Fig. 1). ΔH is related

459 with the velocity in the slot and h_0 with the volume of the pool, therefore different non-uniform
460 situations are likely to produce different turbulence and velocity fields, either in the same pool
461 during different scenarios (Fig. 7 and 8) or between different pools during the same scenario
462 (Fig. 10). This work confirms this fact by demonstrating the importance of considering the
463 influence of river variability in the form of non-uniform boundary conditions for the hydraulic
464 and biological analysis of fishways.

465 Fig. 10 shows the u distribution for the two studied pools during the two considered scenarios.
466 A structure without slope, such as the model used in this work provides a suitable example to
467 illustrate the effects of non-uniformity from a classical 1D perspective. To move the water from
468 one pool to the next it is necessary a water drop, which leads to a reduction of the water level
469 from one pool to the next. Considering that the flow is constant, and that useful area to move
470 to the next pool is reduced [h_0 decreases from pool to pool, M2 profile (Fig. 1)] and invoking
471 the continuity equation ($Q = u \cdot \text{Area} = u \cdot b \cdot h_0$), as we move forward this will produce a progres-
472 sive increment of the velocity in the slot (c.f. vertical profiles in Fig. 10) and an increase of the
473 drop between pools. In the presence of a slope, another two profiles are possible (Rajaratnam
474 et al., 1986): A uniform profile, which is usually the reference case, is produced when the fish-
475 way is in geometrical and hydraulic equilibrium, and the M1 profile, which generates the con-
476 trary effect of M2, a progressive increment of h_0 and a reduction of the water drop and velocity
477 in the slots.

478 It is also necessary to consider that non-uniformity between pools is also generated by geomet-
479 rical deviations (Fuentes-Pérez et al., 2014; Marriner et al., 2016) or local hydraulic effects, e.g.
480 changes in the flow rates into and out of the fishway. In this sense, entrances and exits are likely
481 to produce flow patterns that may alter the performance of a pool assumed to be working in
482 equilibrium, that is to say, a pool surrounded by other pools. Eliminating the influence of these
483 in fishway studies may be nearly impossible as a fish is going to be also subject to these condi-
484 tions.



486 **Fig. 10.** Simulated non-uniform u profiles (parallel to the bed at a height $0.60 \cdot h_{0,2}$ and vertical at 1.30 m
 487 from the right wall) of the laboratory model of the VSF in Koblenz using LES method. a) $Q = 0.170$
 488 m^3/s with a $h_{2,3}$ of 0.46 m. b) $Q = 0.130 \text{ m}^3/\text{s}$ with a $h_{2,3}$ of 0.40 m. (2 columns)

489 Regarding the velocity, local hydraulic variability will change the velocities between scenarios
 490 [Fig. 10(b) against Fig. 10(a)] and between pools in the same scenario. This fact has direct
 491 consequences for fish. Fish need to be able to swim faster than observed velocities in the slot
 492 for moving upstream, and to make this possible fishways are usually designed considering uni-
 493 form conditions and the burst speed of fish (highest speed attainable and maintainable for a
 494 short period of time) (FAO/DVWK, 2002; Katopodis, 1992; Larinier, 2002b). Therefore, M2

495 profiles, which increase velocities and drops in the most downstream slot, may lead to impass-
496 able scenarios. In other cases, lower drops and velocity profiles in the most downstream slots
497 (such as the ones generate by M1 profiles) may reduce the attraction and localization of the
498 fishway entrance.

499 Regarding turbulence, Figs. 7 and 8 shows that it is also highly affected in magnitude and spatial
500 distribution by non-uniformity, and it may affect fish in different ways. Indeed, turbulence has
501 been deemed as a twofold regarding its impact on fish swimming capacity and behaviour. It has
502 been postulated that high turbulence can decrease swimming performance (Lupandin, 2005)
503 and increase the cost of swimming performance (Enders et al., 2005; Guiny et al., 2005). Fish
504 have also exhibiting preferences for low turbulence regions within fishways (Duarte and
505 Ramos, 2012; Silva et al., 2012, 2011) and in general high turbulence levels seems to affect
506 negatively fishway passage (Mallen-Cooper et al., 2008).

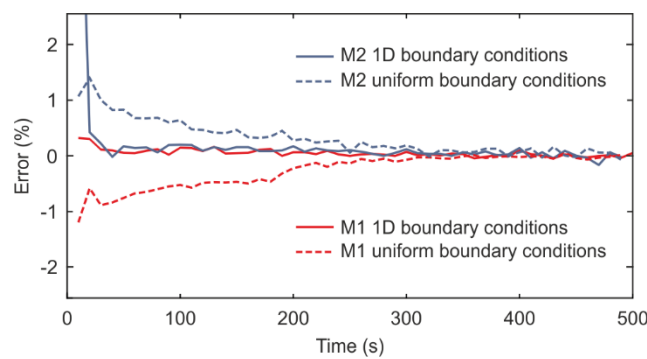
507 However, turbulence is not intrinsically costly and might be controlled to enhance the passage
508 efficiency (Castro-Santos et al., 2009; Tarrade et al., 2011). For instance, by controlling or de-
509 signing structures that provide vortices of a specific size and periodicity inside the pool (Liao,
510 2004). In order to study the spatial distribution of turbulence 3D models provide a necessary
511 tool to relate the possible effect of non-uniformity and design specific solutions.

512 **5.3. 1D against 3D models**

513 1D model are based in the resolution of two equations (Eqs. 1 and 2) for each cross-wall (Fig.
514 2), thus they offer an instantaneous convergence to a solution. Nevertheless, the characteriza-
515 tion of the performance using 1D model is limited to predict the water level distribution, u_{max}
516 and VPD (Section 2.1). Although these have been the classical parameters to evaluate the suit-
517 ability for fish fauna (FAO/DVWK, 2002; Larinier, 2002c), they have several limitations. For
518 instance, VPD assumes a mean dissipated turbulence value for a whole pool, omitting the tur-
519 bulence structure and making possible to reach results within the recommenced limits
520 (FAO/DVWK, 2002; Larinier, 2002b) but with inadequate dimensions for fish passage (e.g.
521 small L and large B) if certain dimensional guidelines are not followed (Larinier, 2002b).

522 In the same way, u_{max} may poorly represent the complexity of the flow over the slot, as in addi-
523 tion to a maximum, there is a minimum and a range of values which may be suitable for the
524 passage of fish fauna (see vertical profile in Fig. 10). Moreover, retrofitting via small geomet-
525 rical changes in the fishway can impact both parameters by reducing the overall turbulence

526 (Mallen-Cooper et al., 2008), modifying turbulence structure or ensuring regions with low ve-
 527 locities (Tarrade et al., 2008). However, these changes cannot be measured or empirically eval-
 528 uated. Fundamentally, as it has been demonstrated, the hydrodynamics of fishways is an amal-
 529 gamation of rapidly occurring 3D flow phenomenon. However, we found that 1D models can
 530 be an interesting tool for a preliminary assessment of well-known design types. In the same
 531 way, they can be used to correctly define the initial conditions within a 3D model and accelerate
 532 its convergence (Fig. 11). As it is shown in the Fig. 11, the use of the calculated water levels in
 533 1D model as water level initial conditions in 3D models reduces the time to reach the asymptotic
 534 region and, in turns, can lead to a reduction the modelling effort and computational cost.



535

536 **Fig. 11.** An example of a water level distribution convergence, showing the influence of the starting
 537 conditions using the design No.3 defined by Rajaratnam et al. (1986) ($\Delta x = 0.06$ m). (1 column)

538 6. Summary and conclusions

539 In the present study, the performance of VSFs under non-uniform condition is modelled and
 540 studied, using OpenFOAM CFD platforms.

541 Two different turbulence modelling techniques have been applied, RANS $k-\epsilon$ and LES-Sma-
 542 gorinsky. Both turbulence models are able to provide acceptable results when compared to la-
 543 boratory velocity measurements, and it was found that the LES model outperformed RANS
 544 when comparing the spatial distributions of the measured velocity data. Taking into account the
 545 strengths and weaknesses of both models, an integrated approach is suggested which may gen-
 546 erate resource-efficient alternatives; using RANS to simulate larger spatial scales correspond-
 547 ing to the time-averaged flow, and LES in regions where a more detailed analysis is required.

548 It was observed that non-uniformity alters the h_0 and ΔH_s profile distributions within a fishway.
 549 Due to their influence on large-scale flow characteristics, the turbulence and velocity fields
 550 were also observed to change in response. This highlights the necessity of considering non-

551 uniformity for the design and evaluation of fishways. It was also found that 3D modelling offers
552 several advantages over classical 1D modelling techniques; 3D models produce a higher level
553 of spatial detail, which can aid in the analysis of the influence of local hydrodynamics and the
554 fish's probability of occurrence in a particular region of the flow field. A major finding of this
555 work is that, 1D models can be very useful to define the boundary conditions of 3D models.

556 We conclude that each method (3D-LES, 3D-RANS and 1D) can be leveraged in synergy to
557 provide time and resource efficient fishway models capable of accurately representing the
558 highly turbulent flows found in vertical slot fishways. The use of each model is study-case
559 dependent, and the use of 1D models to first determine the basic operational conditions, con-
560 sidering non-uniformity is highly encouraged before 3D modelling is applied.

561 **7. Acknowledgments**

562 Authors will like to thank the two anonymous reviewer for their constructive inputs and sug-
563 gestions to the first version of the manuscript. This project has received funding from the Eu-
564 ropean Union's Horizon 2020 research and innovation programme under grant agreement No
565 727830, FITHydro. The research leading to these results has received funding from BONUS
566 (FishView), the joint Baltic Sea research and development programme (Art 185), funded jointly
567 from the European Union's Seventh Programme for research, technological development and
568 demonstration and from the Academy of Finland (under the Grant No. 280715), the German
569 Federal Ministry for Education and Research (BMBFFKZ:03F0687A), and the Estonian Envi-
570 ronmental Investment Centre (KIK P.7254 C.3255). Juan Francisco Fuentes-Perez has also
571 been partly financed by the EU FP7 project ROBOCADEMY (No.608096). Ana T. Silva was
572 financed by the SafePass project (no. 244022) funded by the Research Council of Norway
573 (RCN) under the ENERGIX program. J. Tuhtan's contribution was financed in part by the Es-
574 tonian base financing grant (B53), Octavo and PUT grant (1690) Bioinspired Flow Sensing.

575 **8. Notation**

576 The following symbols are used in this paper:

577 B = pool width (m)

578 b = slot width (m)

579 C_V = Villemonte discharge coefficient (dimensionless)

580 C_ν = standard $k-\epsilon$ turbulent model coefficient (dimensionless)

581 C_l = standard $k-\epsilon$ turbulent model coefficient (dimensionless)

582	C_2	=	standard k - ε turbulent model coefficient (dimensionless)
583	C_k	=	Smagorinsky turbulent model coefficient (dimensionless)
584	C_e	=	Smagorinsky turbulent model coefficient (dimensionless)
585	Cr	=	Courant number (dimensionless)
586	C_s	=	Smagorinsky constant (dimensionless)
587	PSD	=	power spectral density [(m ² s ⁻²) /Hz]
588	g	=	acceleration due to gravity (m/s ²)
589	H	=	total height of the transversal obstacle (m)
590	h_0	=	mean water level of the flow in the pool (m)
591	h_1	=	mean water level of the flow in the pool upstream of the cross-wall (m)
592	h_2	=	mean water level of the flow in the pool downstream of the cross-wall (m)
593	k	=	turbulence kinetic energy (m ² /s ² = J/kg)
594	L	=	pool length (m)
595	p	=	pressure (Pa)
596	Q	=	discharge or flow rate (m ³ /s)
597	R^2	=	determination coefficient (dimensionless)
598	S_{ij}	=	rate of strain (s ⁻¹)
599	I	=	turbulence intensity (dimensionless)
600	t	=	time (s)
601	u	=	velocity (m/s)
602	u'	=	velocity fluctuations (m/s)
603	u_c	=	compression velocity (m/s)
604	u_{max}	=	maximum velocity (m/s)
605	$u_i u_j u_k$	=	velocity components (m/s)
606	VPD	=	volumetric power dissipation (W/m ³)
607	$x_i x_j x_k$	=	Cartesian coordinates (m)
608	β_0, β_1	=	Villemonte's equation coefficients (dimensionless)
609	Δ	=	filter width (m)
610	ΔH	=	water level difference between pools or head drop ($\Delta H = h_1 - h_2$) (m)
611	Δx	=	size of cubic element (m)
612	ΔZ	=	topographic difference between cross-walls (m)
613	α	=	volume fraction
614	σ_k	=	standard k - ε turbulent model coefficient (dimensionless)
615	σ_ε	=	standard k - ε turbulent model coefficient (dimensionless)

616	ε	=	turbulence dissipation rate ($\text{m}^2/\text{s}^3 = \text{J}/(\text{kg}\cdot\text{s})$)
617	ρ	=	density of water (kg/m^3)
618	ν	=	kinematic viscosity (m^2/s)
619	ν_{eff}	=	effective viscosity (m^2/s)
620	ν_t	=	turbulent kinematic viscosity (m^2/s)
621	ν_{sgs}	=	subgrid-scale kinematic viscosity (m^2/s)
622	ω	=	vorticity (s^{-1})
623	τ	=	Reynolds stress (N/m^2)
624	ϕ	=	auxiliary symbol for representing other fluid properties
625			

626 9. References

- 627 An, R., Li, J., Liang, R., Tuo, Y., 2016. Three-dimensional simulation and experimental study
628 for optimising a vertical slot fishway. *J. Hydro-environment Res.* 12, 119–129.
- 629 Barton, A.F., Keller, R.J., 2003. 3D free surface model for a vertical slot fishway, in:
630 *Proceedings of the XXX IAHR Congress, AUTH, Thessaloniki, Greece.*
- 631 Barton, A.F., Keller, R.J., Katopodis, C., 2009. Verification of a numerical model for the
632 prediction of low slope vertical slot fishway hydraulics. *Aust. J. Water Resour.* 13, 53–60.
633 doi:10.1080/13241583.2009.11465360
- 634 Bayon, A., Valero, D., García-Bartual, R., López-Jiménez, P.A., 2016. Performance assessment
635 of OpenFOAM and FLOW-3D in the numerical modeling of a low Reynolds number
636 hydraulic jump. *Environ. Model. Softw.* 80, 322–335. doi:10.1016/j.envsoft.2016.02.018
- 637 Berberović, E., van Hinsberg, N.P., Jakirlić, S., Roisman, I. V, Tropea, C., 2009. Drop impact
638 onto a liquid layer of finite thickness: Dynamics of the cavity evolution. *Phys. Rev. E* 79,
639 36306. doi:10.1103/PhysRevE.79.036306
- 640 Bermúdez, M., Puertas, J., Cea, L., Pena, L., Balairón, L., 2010. Influence of pool geometry on
641 the biological efficiency of vertical slot fishways. *Ecol. Eng.* 36, 1355–1364.
642 doi:10.1016/j.ecoleng.2010.06.013
- 643 Bice, C.M., Zampatti, B.P., Mallen-Cooper, M., 2017. Paired hydraulically distinct vertical-slot
644 fishways provide complementary fish passage at an estuarine barrier. *Ecol. Eng.* 98, 246–
645 256. doi:10.1016/j.ecoleng.2016.11.001
- 646 Blocken, B., Gualtieri, C., 2012. Ten iterative steps for model development and evaluation
647 applied to Computational Fluid Dynamics for Environmental Fluid Mechanics. *Environ.*
648 *Model. Softw.* 33, 1–22. doi:10.1016/j.envsoft.2012.02.001
- 649 Bombač, M., Novak, G., Rodič, P., Četina, M., 2014. Numerical and physical model study of a
650 vertical slot fishway. *J. Hydrol. Hydromechanics* 62, 150–159. doi:10.2478/johh-2014-
651 0013

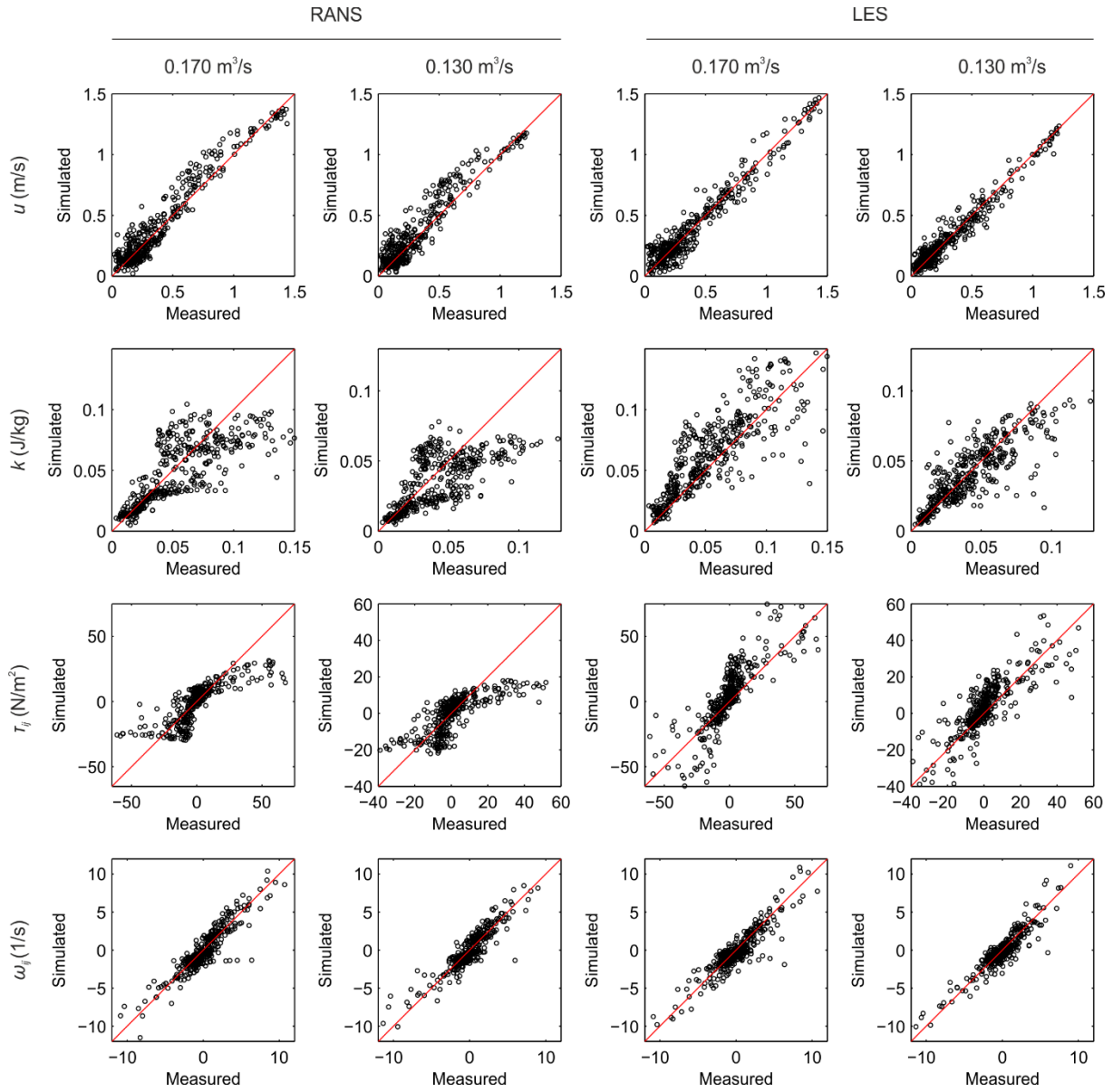
- 652 Branco, P., Segurado, P., Santos, J.M., Pinheiro, P., Ferreira, M.T., 2012. Does longitudinal
653 connectivity loss affect the distribution of freshwater fish? *Ecol. Eng.* 48, 70–78.
654 doi:10.1016/j.ecoleng.2011.05.008
- 655 Castro-Santos, T., Cotel, A., Webb, P.W., 2009. Fishway evaluations for better bioengineering:
656 an integrative approach, in: *Challenges for Diadromous Fishes in a Dynamic Global*
657 *Environment*. American Fisheries Society, Symposium. pp. 557–575.
- 658 Cea, L., Pena, L., Puertas, J., Vázquez-Cendón, M.E., Peña, E., 2007. Application of several
659 depth-averaged turbulence models to simulate flow in vertical slot fishways. *J. Hydraul.*
660 *Eng.* 133, 160–172. doi:10.1061/(ASCE)0733-9429(2007)133:2(160)
- 661 Celik, I., Klein, M., Janicka, J., 2009. Assessment measures for engineering LES applications.
662 *J. Fluids Eng.* 131, 31102. doi:10.1115/1.3059703
- 663 Celik, I.B., Ghia, U., Roache, P.J., 2008. Procedure for estimation and reporting of uncertainty
664 due to discretization in CFD applications. *J. Fluids Eng.* 130, 78001.
665 doi:10.1115/1.2960953
- 666 Clay, C.H., 1995. *Design of fishways and other fish facilities*. CRC Press, Ottawa, Canada.
- 667 Deardorff, J.W., 1970. A numerical study of three-dimensional turbulent channel flow at large
668 Reynolds numbers. *J. Fluid Mech.* 41, 453–480. doi:10.1017/S0022112070000691
- 669 Duarte, B.A. de F., Ramos, I.C.R., 2012. Reynolds shear-stress and velocity: positive biological
670 response of neotropical fishes to hydraulic parameters in a vertical slot fishway. *Neotrop.*
671 *Ichthyol.* 10, 813–819. doi:10.1590/S1679-62252012000400014
- 672 Enders, E.C., Boisclair, D., Roy, A.G., 2005. A model of total swimming costs in turbulent
673 flow for juvenile Atlantic salmon (*Salmo salar*). *Can. J. Fish. Aquat. Sci.* 62, 1079–1089.
674 doi:10.1139/f05-007
- 675 Enders, E.C., Boisclair, D., Roy, A.G., 2003. The effect of turbulence on the cost of swimming
676 for juvenile Atlantic salmon (*Salmo salar*). *Can. J. Fish. Aquat. Sci.* 60, 1149–1160.
677 doi:10.1139/f03-101
- 678 FAO/DVWK, 2002. *Fish Passes: Design, Dimensions, and Monitoring*. FAO, Rome, Italy.
- 679 Fuentes-Pérez, J.F., García-Vega, A., Sanz-Ronda, F.J., Martínez de Azagra-Paredes, A., 2017.
680 Villemonte's approach: validation of a general method for modeling uniform and non-
681 uniform performance in stepped fishways. *Knowl. Manag. Aquat. Ecosyst.* 418, 11.
682 doi:10.1051/kmae/2017013
- 683 Fuentes-Pérez, J.F., Sanz-Ronda, F.J., Martínez de Azagra-Paredes, A., García-Vega, A.,
684 Martínez de Azagra, A., García-Vega, A., 2016. Non-uniform hydraulic behavior of pool-
685 weir fishways: a tool to optimize its design and performance. *Ecol. Eng.* 86, 5–12.
686 doi:10.1016/j.ecoleng.2015.10.021
- 687 Fuentes-Pérez, J.F., Sanz-Ronda, F.J., Martínez de Azagra Paredes, A., García-Vega, A., 2014.
688 Modeling Water-Depth Distribution in Vertical-Slot Fishways under Uniform and
689 Nonuniform Scenarios. *J. Hydraul. Eng.* 140, 6014016. doi:10.1061/(ASCE)HY.1943-
690 7900.0000923

- 691 Furbo, E., 2010. Evaluation of RANS turbulence models for flow problems with significant
692 impact of boundary layers. Uppsala University, Sweden.
- 693 Goettel, M.T., Atkinson, J.F., Bennett, S.J., 2015. Behavior of western blacknose dace in a
694 turbulence modified flow field. *Ecol. Eng.* 74, 230–240.
695 doi:10.1016/j.ecoleng.2014.10.012
- 696 Goring, D.G., Nikora, V.I., 2002. Despiking acoustic Doppler velocimeter data. *J. Hydraul.*
697 *Eng.* 128, 117–126.
- 698 Greenshields, C.J., 2015. OpenFOAM: The open source CFD Toolbox. OpenFOAM
699 Foundation Ltd.
- 700 Guiny, E., Ervine, D.A., Armstrong, J.D., 2005. Hydraulic and biological aspects of fish passes
701 for Atlantic salmon. *J. Hydraul. Eng.* 131, 542–553. doi:10.1061/(ASCE)0733-
702 9429(2005)131:7(542)
- 703 Higuera, P., Lara, J.L., Losada, I.J., 2013. Realistic wave generation and active wave absorption
704 for Navier–Stokes models: Application to OpenFOAM®. *Coast. Eng.* 71, 102–118.
705 doi:10.1016/j.coastaleng.2012.07.002
- 706 Hirt, C.W., Nichols, B.D., 1981. Volume of fluid (VOF) method for the dynamics of free
707 boundaries. *J. Comput. Phys.* 39, 201–225. doi:10.1016/0021-9991(81)90145-5
- 708 Jackson, A., 2012. A comprehensive tour of snappyHexMesh, in: 7th OpenFOAM Workshop
709 Lecture. Darmstadt, Germany.
- 710 Katopodis, C., 1992. Introduction to fishway design. *Oceans* 67.
- 711 Khan, L.A., 2006. A three-dimensional computational fluid dynamics (CFD) model analysis of
712 free surface hydrodynamics and fish passage energetics in a vertical-slot fishway. *North*
713 *Am. J. Fish. Manag.* 26, 255–267. doi:10.1577/M05-014.1
- 714 Klein, J., Oertel, M., 2015. Comparison between crossbar block ramp and vertical slot fish pass
715 via numerical 3D simulation, in: 36th IAHR World Congress. The Hague, the Netherlands.
- 716 Krüger, F., Heimerl, S., Seidel, F., Lehmann, B., 2010. Ein Diskussionsbeitrag zur
717 hydraulischen Berechnung von Schlitzpässen. *WasserWirtschaft* 3, 31–36.
718 doi:10.1007/BF03241596
- 719 Larinier, M., 2002a. Location of fishways. *Bull. Fr. Pêche Piscic.* 364, 39–53.
720 doi:10.1051/kmae/2002106
- 721 Larinier, M., 2002b. Pool fishways, pre-barrages and natural bypass channels. *Bull. Fr. Pêche*
722 *Piscic.* 364, 54–82. doi:10.1051/kmae/2002108
- 723 Larinier, M., 2002c. Biological factors to be taken into account in the design of fishways, the
724 concept of obstructions to upstream migration. *Bull. Fr. Pêche Piscic.* 364, 28–38.
725 doi:10.1051/kmae/2002105
- 726 Launder, B.E., Spalding, D.B., 1974. The numerical computation of turbulent flows. *Comput.*
727 *Methods Appl. Mech. Eng.* 3, 269–289. doi:10.1016/0045-7825(74)90029-2

- 728 Liao, J.C., 2004. Neuromuscular control of trout swimming in a vortex street: implications for
729 energy economy during the Karman gait. *J. Exp. Biol.* 207, 3495–3506.
730 doi:10.1242/jeb.01125
- 731 Lilly, D.K., 1966. The representation of small scale turbulence in numerical simulation
732 experiments. National Center for Atmospheric Research, Boulder, Colorado, USA.
733 doi:10.5065/D62R3PMM
- 734 Lopes, P., Tabor, G., Carvalho, R.F., Leandro, J., 2016. Explicit calculation of natural aeration
735 using a Volume-of-Fluid model. *Appl. Math. Model.* 40, 7504–7515.
736 doi:10.1016/j.apm.2016.03.033
- 737 Lupandin, A.I., 2005. Effect of flow turbulence on swimming speed of fish. *Biol. Bull.* 32, 461–
738 466. doi:10.1007/s10525-005-0125-z
- 739 Mallen-Cooper, M., Zampatti, B.P., Stuart, I.G., Baumgartner, L.J., 2008. Innovative Fishways-
740 Manipulating turbulence in the vertical-slot design to improve performance and reduce
741 cost. Fishway Consulting Services, Sydney, Australia.
- 742 Marriner, B.A., Baki, A.B.M., Zhu, D.Z., Cooke, S.J., Katopodis, C., 2016. The hydraulics of
743 a vertical slot fishway: A case study on the multi-species Vianney-Legendre fishway in
744 Quebec, Canada. *Ecol. Eng.* 90, 190–202. doi:10.1016/j.ecoleng.2016.01.032
- 745 Marriner, B.A., Baki, A.B.M., Zhu, D.Z., Thiem, J.D., Cooke, S.J., Katopodis, C., 2014. Field
746 and numerical assessment of turning pool hydraulics in a vertical slot fishway. *Ecol. Eng.*
747 63, 88–101. doi:10.1016/j.ecoleng.2013.12.010
- 748 Mooney, K., Papper, J., Voskuilen, T., 2014. Performance evaluation of existing and new VoF
749 simulation techniques: solving, interface treatment, and dynamic meshes, in: 9th
750 OpenFOAM® Workshop. Zagreb, Croatia, pp. 23–26.
- 751 Moukalled, F., Mangani, L., Darwish, M., 2016. The Finite Volume Method in Computational
752 Fluid Dynamics. Springer. doi:10.1007/978-3-319-16874-6
- 753 Musall, M., Oberle, P., Carbonell-Baeza, R., Fuentes-Pérez, J.F., Tuhtan, J.A., Nestmann, F.,
754 2015. Beitrag zu detaillierten Analysen der Hydraulik von Schlitzpässen.
755 *WasserWirtschaft* 7/8, 67–71. doi:10.1007/s35147-015-0551-x
- 756 NEXT Foam, 2014. Boundary Conditions - OpenFOAM-2.3.0.
- 757 Nilsson, C., Reidy, C.A., Dynesius, M., Revenga, C., 2005. Fragmentation and flow regulation
758 of the world's large river systems. *Science* 308, 405–408. doi:10.1126/science.1107887
- 759 Oberle, P., Musall, M., Riesterer, J., Nestmann, F., 2012. Numerische Modelluntersuchungen
760 im Rahmen der Planung der Fischeaufstiegsanlage Geesthacht. *WasserWirtschaft* 102, 28–
761 33. doi:10.1365/s35147-012-0243-8
- 762 Odeh, M., Noreika, J., Haro, A., Maynard, A., Castro-Santos, T., Cada, G.F., 2002. Evaluation
763 of the effects of turbulence on the behavior of migratory fish. Final Report 2002, Report
764 to Bonneville Power Administration, Contract No. 00000022, Project No. 200005700.
765 Portland, Oregon, USA.

- 766 Openfoam, 2016. Standard boundary conditions [WWW Document]. URL
 767 <http://www.openfoam.com/documentation/user-guide/standard-boundaryconditions.php>
 768 (accessed 10.2.16).
- 769 Poleni, G., 1717. De motu aquae mixto libri duo, Padova: G.Comini; VII, 132 p.; in 8.;
 770 DCC.4.24. Iosephi Comini, Patavii.
- 771 Pope, S.B., 2001. Turbulent flows. Meas. Sci. Technol. 12, 2020. doi:10.1088/0957-
 772 0233/12/11/705
- 773 Puertas, J., Cea, L., Bermúdez, M., Pena, L., Rodríguez, Á., Rabuñal, J.R., Balairón, L., Lara,
 774 Á., Aramburu, E., 2012. Computer application for the analysis and design of vertical slot
 775 fishways in accordance with the requirements of the target species. Ecol. Eng. 48, 51–60.
 776 doi:10.1016/j.ecoleng.2011.05.009
- 777 Puertas, J., Pena, L., Teijeiro, T., 2004. Experimental approach to the hydraulics of vertical slot
 778 fishways. J. Hydraul. Eng. 130, 10–23. doi:10.1061/(ASCE)0733-9429(2004)130:1(10)
- 779 Quaranta, E., Comoglio, C., Christos, K., Roberto, R., 2016. Numerical simulations of flow
 780 field in vertical slot fishways.
- 781 Rajaratnam, N., Katopodis, C., Mainali, A., 1989. Pool-orifice and pool-orifice-weir fishways.
 782 Can. J. Civ. Eng. 16, 774–777. doi:10.1139/189-112
- 783 Rajaratnam, N., Katopodis, C., Solanki, S., 1992. New designs for vertical slot fishways. Can.
 784 J. Civ. Eng. 19, 402–414. doi:10.1139/192-049
- 785 Rajaratnam, N., Van der Vinne, G., Katopodis, C., 1986. Hydraulics of vertical slot fishways.
 786 J. Hydraul. Eng. 112, 909–927. doi:10.1061/(ASCE)0733-9429(1986)112:10(909)
- 787 Sidebottom, W., Ooi, A., Jones, D., 2015. A Parametric Study of Turbulent Flow Past a Circular
 788 Cylinder Using Large Eddy Simulation. J. Fluids Eng. 137, 91202. doi:10.1115/1.4030380
- 789 Silva, A.T., Katopodis, C., Santos, J.M., Ferreira, M.T., Pinheiro, A.N., 2012. Cyprinid
 790 swimming behaviour in response to turbulent flow. Ecol. Eng. 44, 314–328.
 791 doi:10.1016/j.ecoleng.2012.04.015
- 792 Silva, A.T., Santos, J.M., Ferreira, M.T., Pinheiro, A.N., Katopodis, C., 2011. Effects of water
 793 velocity and turbulence on the behaviour of Iberian barbel (*Luciobarbus bocagei*,
 794 Steindachner 1864) in an experimental pool-type fishway. River Res. Appl. 27, 360–373.
 795 doi:10.1002/rra.1363
- 796 Smagorinsky, J., 1963. General circulation experiments with the primitive equations: I. the
 797 basic experiment. Mon. Weather Rev. 91, 99–164. doi:10.1175/1520-
 798 0493(1963)091<0099:GCEWTP>2.3.CO;2
- 799 Tarrade, L., Pineau, G., Calluau, D., Texier, A., David, L., Larinier, M., 2011. Detailed
 800 experimental study of hydrodynamic turbulent flows generated in vertical slot fishways.
 801 Environ. fluid Mech. 11, 1–21. doi:10.1007/s10652-010-9198-4
- 802 Tarrade, L., Texier, A., David, L., Larinier, M., 2008. Topologies and measurements of
 803 turbulent flow in vertical slot fishways. Hydrobiologia 609, 177–188.

- 804 doi:10.1007/s10750-008-9416-y
- 805 Ubbink, O., 1997. Numerical prediction of two fluid systems with sharp interfaces. University
806 of London, London, UK.
- 807 Van Balen, W., Blanckaert, K., Uijttewaal, W.S.J., 2010. Analysis of the role of turbulence in
808 curved open-channel flow at different water depths by means of experiments, LES and
809 RANS. *J. Turbul.* 11, N12. doi:10.1080/14685241003789404
- 810 Villemonte, J.R., 1947. Submerged-weir discharge studies. *Eng. News-Record* 139, 866–869.
- 811 Von Kármán, T.H., 1931. Mechanical similitude and turbulence. National Advisory Committee
812 on Aeronautics, Washington, USA.
- 813 Vuorinen, V., Chaudhari, A., Keskinen, J.-P., 2015. Large-eddy simulation in a complex hill
814 terrain enabled by a compact fractional step OpenFOAM® solver. *Adv. Eng. Softw.* 79,
815 70–80. doi:10.1016/j.advengsoft.2014.09.008
- 816 Wahl, T.L., 2003. Discussion of “Despiking acoustic doppler velocimeter data” by Derek G.
817 Goring and Vladimir I. Nikora. *J. Hydraul. Eng.* 129, 484–487.
- 818 Weller, H.G., Tabor, G., Jasak, H., Fureby, C., 1998. A tensorial approach to computational
819 continuum mechanics using object-oriented techniques. *Comput. Phys.* 12, 620–631.
820 doi:10.1063/1.168744
- 821 Wu, S., Rajaratnam, N., Katopodis, C., 1999. Structure of flow in vertical slot fishway. *J.*
822 *Hydraul. Eng.* 125, 351–360. doi:10.1061/(ASCE)0733-9429(1999)125:4(351)
- 823 Xu, T., Sun, S., 2009. Numerical simulation of the flow structure in vertical slot fishway, in:
824 33rd IAHR Congress: Water Engineering for a Sustainable Environment. International
825 Association of Hydraulic Engineering & Research (IAHR), Vancouver, Canada.
- 826 Zhang, J., Tejada-Martínez, A.E., Zhang, Q., 2014. Developments in computational fluid
827 dynamics-based modeling for disinfection technologies over the last two decades: A
828 review. *Environ. Model. Softw.* 58, 71–85. doi:10.1016/j.envsoft.2014.04.003
- 829



832

833 **Fig. S1.** Distribution of the measured point against simulated points for u , k , τ_{ij} and ω_{ij} for all the studied
 834 scenarios and turbulence model. Table 4 shows a numerical summary of the figure.

835

836